



HAL
open science

Atmospheric mercury speciation dynamics at the high-altitude Pic du Midi Observatory, southern France

X. Fu, N. Maruszczak, Lars-Eric Heimbürger-Boavida, B. Sauvage, F. Gheusi, E. Prestbo, E. Sonke

► To cite this version:

X. Fu, N. Maruszczak, Lars-Eric Heimbürger-Boavida, B. Sauvage, F. Gheusi, et al.. Atmospheric mercury speciation dynamics at the high-altitude Pic du Midi Observatory, southern France. *Atmospheric Chemistry and Physics*, 2016, pp.1-35. 10.5194/acp-2015-842 . hal-02163095

HAL Id: hal-02163095

<https://hal.science/hal-02163095>

Submitted on 22 Jan 2020

HAL is a multi-disciplinary open access archive for the deposit and dissemination of scientific research documents, whether they are published or not. The documents may come from teaching and research institutions in France or abroad, or from public or private research centers.

L'archive ouverte pluridisciplinaire **HAL**, est destinée au dépôt et à la diffusion de documents scientifiques de niveau recherche, publiés ou non, émanant des établissements d'enseignement et de recherche français ou étrangers, des laboratoires publics ou privés.



Distributed under a Creative Commons Attribution 4.0 International License



1 Atmospheric mercury speciation dynamics at the high-altitude Pic du Midi
2 Observatory, southern France

3
4 X. W. Fu^{1,2}, N. Maruszczak¹, L.-E. Heimbürger^{1,3}, B. Sauvage⁴, F. Gheusi⁴, E. M.
5 Prestbo⁵, J. E. Sonke¹,

6 ¹Observatoire Midi-Pyrénées, Laboratoire Géosciences Environnement Toulouse, CNRS/IRD/Université de
7 Toulouse, 14, avenue Édouard Belin, 31400 Toulouse, France

8 ²State Key Laboratory of Environmental Geochemistry, Institute of Geochemistry, Chinese Academy of Sciences,
9 Guiyang, China.

10 ³Mediterranean Institute of Oceanography, Campus de Luminy, 13288 Marseille, France

11 ⁴Observatoire Midi-Pyrénées, Laboratoire d'Aérodologie, CNRS/IRD/Université de Toulouse, 14, avenue Édouard
12 Belin, 31400 Toulouse, France

13 ⁵Tekran Research and Development, 330 Nantucket Blvd., Toronto, ON, Canada M1P2P4

14 Correspondence to: *Xuewu Fu E-mail : fuxuewu@mail.gyig.ac.cn

15



16 Abstract: Continuous measurements of atmospheric gaseous elemental mercury (GEM),
17 particulate bound mercury (PBM) and gaseous oxidized mercury (GOM) at the high-altitude Pic
18 du Midi Observatory (PDM, 2877 m a.s.l) in southern France were made from Nov 2011 to Nov
19 2012. The mean GEM, PBM and GOM concentrations were 1.86 ng m^{-3} , 14 pg m^{-3} and 27 pg m^{-3} ,
20 respectively and we observed 44 high PBM (up to 98 pg m^{-3}) and 61 high GOM (up to 295 pg m^{-3})
21 events. The high PBM events occurred mainly in cold seasons (winter and spring) whereas high
22 GOM events were mainly observed in the warm seasons (summer and autumn). In cold seasons
23 the maximum air mass residence times (ARTs) associated with high PBM events were observed in
24 the upper troposphere over North America. The ratios of high PBM ARTs to total ARTs over North
25 America, Europe, the Arctic region and Atlantic Ocean were all elevated in the cold season
26 compared to the warm season, indicating that the middle and upper free troposphere of the
27 Northern Hemisphere may be more enriched in PBM in cold seasons. PBM concentrations and
28 PBM/GOM ratios during the high PBM events were significantly anti-correlated with atmospheric
29 aerosol concentrations, air temperature and solar radiation, suggesting in situ formation of PBM in
30 the middle and upper troposphere. We identified two distinct types of high GOM events with the
31 GOM concentrations positively and negatively correlated with atmospheric ozone concentrations,
32 respectively. High GOM events positively correlated with ozone were mainly related to air masses
33 from the upper troposphere over the Arctic region and middle troposphere over the temperate
34 North Atlantic Ocean, whereas high GOM events anti-correlated with ozone were mainly related
35 to air masses from the lower free troposphere over the subtropical North Atlantic Ocean. The
36 ARTs analysis demonstrates that the lower and middle free troposphere over the North Atlantic
37 Ocean was the largest source region of atmospheric GOM at PDM Observatory. The ratios of high
38 GOM ARTs to total ARTs over the subtropical North Atlantic Ocean in summer were significantly
39 higher than that over the temperate and sub-arctic North Atlantic Ocean as well as that over the
40 North Atlantic Ocean in other seasons, indicating abundant in situ oxidation of GEM to GOM in
41 the lower free troposphere over the subtropical North Atlantic Ocean in summer.
42



43 1 Introduction

44 Transformations of mercury (Hg) in the atmosphere play a crucial role in the global Hg cycle
45 (Selin et al., 2007; Driscoll et al., 2013). Gaseous elemental mercury (GEM) is the predominant
46 form emitted by anthropogenic and natural sources (Pirrone et al., 2010). GEM is then
47 transformed to gaseous oxidized mercury (GOM) and particulate bound mercury (PBM) by
48 oxidation. Atmospheric Hg deposition occurs by wet deposition and dry deposition pathways.
49 Models suggest global GEM dry deposition to be potentially important, yet lack broad
50 observational evidence (Selin et al., 2008). On the other hand, GOM and PBM are readily
51 scavenged from the atmosphere by cloud droplets followed by wet deposition, and by dry
52 deposition. Hence, conversion of GEM to GOM and PBM is a crucial process in the removal of
53 Hg in the atmosphere, which in turn affects the loading of Hg to terrestrial and marine ecosystems.

54 Conversion of GEM to GOM and PBM is potentially occurring throughout the global
55 atmosphere, but the rates of conversion are thought to vary and are dependent on the levels of
56 atmospheric oxidants and environmental factors. Current modeling studies suggested that
57 conversion of GEM to GOM and PBM produces approximate 8000 tons of GOM and PBM
58 annually, which explains at least 90% of the total sources of GOM and PBM in the atmosphere
59 (Holmes et al., 2010). However, it is still unclear where the majority of the conversion takes place,
60 by what mechanism and what the major oxidants and environmental factors are involved. Over the
61 last decade, studies have been carried out to measure atmospheric Hg speciation at high-altitude
62 sites in the USA and Asia and on research flights. A study at the Mount Bachelor observatory
63 (MBO, USA) showed elevated GOM (up to 600 pg m⁻³) and low GEM in the free troposphere,
64 suggesting in situ oxidation (Swartzendruber et al., 2006). Observations at Storm Peak laboratory
65 (SPL, USA) and Lulin Atmospheric Background Station (LABS, Taiwan) showed similar, though
66 less elevated, GOM events in free tropospheric air masses (Fain et al., 2009; Sheu et al., 2010).
67 Long-term Hg speciation observations at MBO suggest GEM oxidation to be enhanced in
68 long-range Asian pollution plumes, but also in marine boundary layer (MBL) air masses
69 originating over the Pacific Ocean (Timonen et al., 2013). INTEX-B in-flight observations of
70 GEM in the tropopause region (8-12km) have shown low GEM levels, sometimes down to zero,
71 indicative of rapid oxidation (Talbot et al., 2007). CARIBIC in-flight observations of total gaseous
72 Hg (TGM ~ GEM+GOM) showed lower TGM levels in the southern hemisphere, TGM depletion
73 in the extratropical lowermost stratosphere and a general positive correlation between TGM and
74 ozone (Slemr et al., 2009; Slemr et al., 2014). In-flight, in-situ analyses of stratospheric aerosols
75 suggest that the upper troposphere and lower stratosphere depletion in GEM is balanced by
76 abundant PBM (Murphy et al., 1998; Murphy et al., 2006). Recent in-flight measurements
77 provided the first simultaneous observations of both GEM and the combined GOM+PBM



78 fractions at an altitude above 6 km (Lyman and Jaffe, 2012). The study showed elevated
79 GOM+PBM levels in stratospheric air masses and confirmed the importance of stratospheric
80 GEM oxidation. The findings of all these studies indicate that the free troposphere and lower
81 stratosphere are important regions for conversion of GEM to GOM and PBM.

82 A recent study reviewed mountain-top studies of free troposphere Hg dynamics and
83 compared observations to the GEOS-Chem atmospheric Hg chemistry and transport
84 model (Weiss-Penzias et al., 2015). The model intercompared Hg oxidation by Br against
85 OH-ozone pathways and was able to only marginally reproduce observations, indicating the need
86 to improve both measurement techniques and models. Additional long-term observations of GEM,
87 GOM, and PBM are therefore necessary to map out regions and altitudes that favor GEM
88 oxidation, and provide insight into the oxidation mechanisms. In the present study, we carried out
89 one year of continuous measurements of speciated atmospheric mercury at the Pic du Midi (PDM)
90 Observatory, a high-altitude site (2877 m a.s.l) in the French Pyrenees mountains. This is the first
91 year-around study of atmospheric Hg speciation at a mid-latitude high-altitude site. This study
92 may help to better understand the seasonal patterns of high GOM and PBM events and the
93 mechanisms underlying the transformations of atmospheric Hg in the free troposphere over the
94 lower, middle and high latitudes.

95

96 **2 Materials and methods**

97 **2.1 Site description**

98 The Pic du Midi (PDM) Observatory (0.142° E, 42.937° N, 2877 m a.s.l) is a high-altitude
99 monitoring station situated on top of an isolated peak (elevated approximately 1300 m relative to
100 the surrounding terrain) on the northern edge of the central Pyrenees mountains, Southwest France.
101 It is approximately 150 km to the east of the North Atlantic coast and 210 km to west of the
102 Mediterranean Sea. The PDM Observatory frequently receives free tropospheric air from the
103 North Atlantic and Europe (Henne et al., 2010). The station may also be partly influenced by
104 boundary layer air transported by plain-to-mountain winds from southwest France or through
105 regional transport from Spain under southerly or south-westerly synoptic wind conditions (Gheusi
106 et al., 2011; Tsamalis et al., 2014). There are no source points around the station or in the
107 surrounding areas. The two nearest cities are Pau and Tarbes which are respectively located 60 and
108 30 km northwest to the station and may influence the observations via upslope transport.

109

110 **2.2 Measurements of speciated atmospheric mercury and Ancillary parameters**

111 Speciated atmospheric Hg is continuously measured at PDM Observatory using the Tekran
112 2537/1130/1135 system (Tekran Inc., Canada). The period analyzed in this study goes from 18th



113 Nov 2011 to 17th Nov 2012. The Tekran system has been widely used and described in detail
114 elsewhere (Landis et al., 2002; Lindberg et al., 2002). Briefly, GOM, PBM, and GEM in ambient
115 air were collected onto KCl-coated annular denuder, regenerable quartz fiber filter and dual gold
116 cartridges in sequence. The system was programmed to collect GOM and PBM at 1-h intervals at
117 a volumetric flow rate of 10 L min⁻¹; and GEM was collected at 5-min intervals at a volumetric
118 flow rate of 1.07 L min⁻¹. Once collected, Hg is thermally decomposed from each unit and
119 detected by cold vapor atomic fluorescence spectroscopy (CVAFS) as Hg⁰. KCl-coated denuder,
120 Teflon coated glass inlet, and impactor plate were replaced bi-weekly and quartz filters were
121 replaced monthly. Denuders and quartz filters were prepared and cleaned before field sampling
122 following the methods in Tekran technical notes. The Tekran 2537B analyzer was routinely
123 calibrated using its internal permeation source at a 47 h interval, and was also cross-calibrated
124 every 3 months against an external temperature controlled Hg vapor standard. Due to the frequent
125 extreme weather conditions at PDM Observatory, the system was installed inside a
126 temperature-controlled laboratory. Ambient air was introduced into the Tekran unit using the
127 Tekran 1004 Teflon coated manifold, which is similar as that used at the MBO,
128 USA (Swartzendruber et al., 2006). The inlet of the Tekran 1104 manifold was about 0.5 m from
129 the outside wall of the laboratory and oriented to the southwest (the local predominant wind
130 direction) of the laboratory. Temperature of the Tekran 1104 manifold was kept at 70 °C and air
131 flow through the manifold was about 100 L min⁻¹. Blanks of Tekran unit and manifold were
132 quantified at the beginning and end of each maintenance (bi-weekly) using Hg-free ambient air.
133 The annual mean GEM blank of the Tekran unit was 0.04 ± 0.03 ng m⁻³ (1SD) and detection limit
134 of GEM was estimated to be 0.1 ng m⁻³.

135 Measurement of GOM and PBM is challenging due to the typical low part per quadrillion
136 (ppq) concentrations, reactivity and potential for species interconversion, and the need to
137 pre-concentrating on a surface. In addition the lack of understanding of the specific forms and
138 accepted calibration standards of GOM and PBM hinders the ability to obtain in-field quality
139 assurance measurements, like dynamic spiking under changing atmospheric conditions. Recently,
140 uncertainties regarding the accuracy of GOM measurements have been discovered related to O₃
141 and water vapor levels suggesting a potential for low GOM bias under certain atmospheric
142 conditions (Lyman et al., 2010; Gustin et al., 2013). Another study using cation exchange
143 membranes suggested that on average KCl-coated denuders may create up to a 50% low bias in
144 the humid air, but was only a comparison of two differing methods, with neither one challenged in
145 real time by standard spiking under atmospheric conditions (Huang et al., 2013). On the other
146 hand, the potential for the PBM to be biased has not been thoroughly studied and understood, for
147 the reasons mentioned above, however the bias would likely be positive due to GEM uptake as the



148 regenerable filter ages and becomes more reactive. At PDM Observatory, similar to other high
149 altitude studies, we do not observe simultaneous increases of PBM during high GOM events
150 suggesting no significant GOM breakthrough or GEM uptake on the filter (Malcolm and Keeler,
151 2007;Swartzendruber et al., 2006;Fain et al., 2009). Similarly GOM loss from denuders has been
152 suggested to relate to high humidity levels (McClure et al., 2014). The elevated free tropospheric
153 PBM and GOM events discussed in this study occur predominantly in low humidity air masses
154 (median humidities of 21 and 28 % respectively) limiting GOM losses. Therefore, as most of the
155 discussion in the present study is based on the relative variations of GOM and PBM, we assume
156 the potential sampling artifacts may bring a minimal uncertainty to the overall findings. Most
157 importantly, the method used in this study and others is “state of the art” at this time and has
158 resulted in profound discoveries that are scientifically coherent (Schroeder and Munthe,
159 1998;Laurier et al., 2003;Lindberg et al., 2002;Swartzendruber et al., 2006;Steffen et al.,
160 2008;Sprovieri et al., 2010;Fu et al., 2015). Currently, there is no better method to routinely
161 separate and quantify low, part-per-quadrillion concentrations of the mercury fractions with hourly
162 time resolution, than the use of a fully heated sample train that rejects large particles(>2.5 μm) by
163 impaction, capture of “sticky” GOM species on a laminar flow, coated annular denuder, which
164 rejects both PBM and GEM, followed by a quartz fiber filter to collect PBM, which rejects GEM
165 so it can pass to a sensitive monitor for continuous detection. The operationally defined method to
166 quantify atmospheric mercury fractions is similar to well established methods used for other
167 “sticky gases” ammonia and nitric acid.

168 Atmospheric CO and ozone concentrations were continuously measured using the TEI
169 48CTL gas filter correlation analyzers and 49C Ozone analyzer (Thermo Environmental
170 Instruments Inc. USA), respectively. Detailed information regarding the principle of the
171 instruments, calibrations, and measurement uncertainties can be found in a previous study (Gheusi
172 et al., 2011).The standard uncertainties associated with CO and ozone datasets (15-min averaged
173 data) were reported to be 6.6 and 1.2 ppbv, respectively (Gheusi et al., 2011). Atmospheric aerosol
174 number concentration in PM₁₀ particles (i.e. of diameter<10 μm) was measured at PDM
175 Observatory using a condensation particle counter (CPC), Model 3010 by TSI Inc. The particles
176 are detected by condensing butanol vapor onto the particles, causing them to grow into droplets.
177 These particles (in the droplet form) are then counted by optical absorption (Gheusi et al., 2011).
178 CO and ozone mole fractions, as well as atmospheric aerosol number concentration and standard
179 meteorological variables at PDM Observatory were obtained as 5-min averages from the PAES
180 (French acronym for atmospheric pollution at synoptic scale; <http://paes.aero.obs-mip.fr/>)
181 network.

182



183 **2.3 Simulations of back trajectories, air masses residence times and potential source regions**

184 In the present study, we calculated 10-day back trajectory for high PBM events and 7-day
185 back trajectory for high GOM events, respectively using the NOAA Hysplit trajectory model and
186 gridded meteorological data (Global Data Assimilation System, GDAS1) (Draxler and Rolph).
187 The GDAS1 has a horizontal resolution of 1 degree (360×180 grid cells) with 23 vertical levels
188 from 1000 hPa to 20 hPa. The trajectories ended at the PDM Observatory at a height of 3000 m
189 a.s.l. (approximately 100 m above the sampling site). In addition, we also used the Flexpart
190 Lagrangian particle dispersion model version 9.0 (Stohl et al., 2005) to simulate the 20 days back
191 trajectories for two special events (high PBM event #12 and #19) and to make a comparison with
192 Hysplit. The Flexpart model is driven by wind fields provided by the European Centre for
193 Medium-range Weather Forecast (ECMWF) with a temporal resolution of 3 hours (analyses at
194 00:00, 06:00, 12:00, 18:00 UTC; forecasts at 03:00, 09:00, 15:00, 21:00 UTC) and with horizontal
195 resolution of 32 km. The model output refers to the time, in seconds, the released particles spent in
196 each output grid box before reaching the PDM Observatory. Flexpart residence times are output
197 every 3 h on a uniform grid of 0.5° latitude × 0.5° longitude in 40 vertical layers from mean sea
198 level to a height of 20 km above sea level. In the present study, we analyzed how air masses from
199 different sublayers in the troposphere affect atmospheric PBM and GOM concentrations at the
200 PDM Observatory. We subdivide the troposphere into 4 sublayers: boundary layer (> 900 hPa),
201 lower free troposphere (700-900 hPa), middle free troposphere (500-700 hPa) and upper free
202 troposphere (200-500 hPa).

203 Air mass residence times (ARTs) were calculated on the basis of the simulations of 7-day
204 backward trajectories ending at PDM Observatory. The studied domain covered by the trajectories
205 was divided into 3590 grid cells of 2.5° latitude × 2.5° longitude. To reduce the “central
206 convergence” effect and highlight the long-range transport processes (Cuevas et al., 2013), we
207 adjusted the residence times using the geometric adjustment factor as proposed by Poirot and
208 Wishinski (1986).

209 The potential source regions of PBM and GOM were simulated using a Potential Source
210 Contribution Function (PSCF) approach (Zeng and Hopke, 1989). The PSCF value indicates the
211 probability that a source area contributed to the receptor site and is defined as:

$$212 \text{PSCF}_{ij} = \frac{M_{ij}}{N_{ij}} \times W_{ij} \quad (1)$$

213 M_{ij} is the total number of endpoints in a grid cell associated to PBM and GOM
214 concentrations at PDM Observatory higher than the annual means, N_{ij} is the total number of
215 endpoints in a grid cell, and W_{ij} is a weighting function used to minimize the uncertainties of a
216 small N_{ij} and described by Polissar et al (2001). For the PBM and GOM PSCF analysis, 7-day
217 back trajectories ending at PDM Observatory were calculated every 2 hours throughout the whole



218 study period. The total trajectory endpoints in the boundary layer, lower free troposphere, and
219 middle and upper troposphere in the studied domain were 152025, 285726, and 250557,
220 respectively. The studied domain was divided into 5566 grid cells of 2.0° latitude \times 2.0° longitude.
221 Areas with high PSCF values are likely enriched in atmospheric PBM and GOM and probably
222 contribute to the elevated PBM and GOM concentrations at PDM Observatory.

223

224 **3 Results and discussion**

225 **3.1 Annual, seasonal, and diel trends**

226 Averaged atmospheric GEM, PBM, and GOM concentrations at PDM Observatory during
227 the study period were 1.86 ± 0.27 ng m⁻³, 14 ± 10 pg m⁻³, and 27 ± 34 pg m⁻³, respectively (time
228 series of GEM, PBM and GOM concentrations are in Figure S1). The level of GEM at PDM
229 Observatory was slightly higher than the previous observations at remote sites in Europe (means:
230 $1.66 - 1.82$ ng m⁻³) (Slemr and Scheel, 1998; Lee et al., 1998; Kock et al., 2005) and North America
231 (means: $1.32 - 1.72$ ng m⁻³) (Kellerhals et al., 2003; Lan et al., 2012), but lower than that observed
232 in Asia (means: $1.60 - 3.98$ ng m⁻³) (Fu et al., 2015). Continuous measurements of atmospheric
233 Hg speciation at high-altitude sites are limited worldwide. The mean PBM concentration at PDM
234 Observatory was approximately 7 times higher than at LABS (2 pg m⁻³, 23.5° N, 2862 m asl)
235 (Sheu et al., 2010), and also higher than the summertime means at SPL (9 pg m⁻³, 40.5° N, 3230 m
236 a.s.l) and MBO (5 pg m⁻³, 44.0° N, 2700 m a.s.l) (Swartzendruber et al., 2006; Fain et al., 2009).
237 The annual mean GOM concentration at PDM Observatory was relatively higher than at LABS
238 (12 pg m⁻³) and SPL (20 pg m⁻³) (Fain et al., 2009; Sheu et al., 2010), but lower than at MBO (40
239 pg m⁻³) (Swartzendruber et al., 2006). The difference in atmospheric PBM and GOM
240 concentrations among high-altitude sites may partially reflect measurements uncertainty, but also
241 be due to the different regional and long-range Hg transport, atmospheric Hg transformations, and
242 intrusions of air from the upper troposphere and lower stratosphere.

243 Differences in GEM concentrations for different seasons were not statistically significant (t
244 test $p = 0.73$, Figure 1). The monthly mean PBM concentrations were relatively higher ($p < 0.05$)
245 in winter (December to February) and spring (March to May) than in summer (June to August)
246 and autumn (September to November), with the highest monthly mean of 21 pg m⁻³ in February
247 and the lowest monthly mean of 7 pg m⁻³ in October. This seasonal pattern is similar to the
248 observations at LABS as well as low-altitude sites in North America and China (Lan et al.,
249 2012; Fu et al., 2012; Sheu et al., 2010). Elevated winter PBM concentrations are common at
250 low-altitude sites in the Northern Hemisphere, which is likely linked to emissions from residential
251 heating, and low temperature facilitating gas-particle partitioning of atmospheric mercury, and
252 decreasing wet scavenging processes (Lan et al., 2012; Rutter and Schauer, 2007; Selin et al., 2007).



253 Monthly mean GOM concentrations were relatively higher ($p < 0.05$) in summer (mean: 38 pg m^{-3}),
254 followed by winter (mean: 25 pg m^{-3}), autumn (mean: 25 pg m^{-3}), and spring (mean: 23 pg m^{-3})
255 (Figure 1). In general, in-situ oxidation of GEM and long-range transport of GOM-enriched air
256 from the free troposphere, rather than anthropogenic emissions are the dominant sources of
257 atmospheric GOM at high-altitude sites (Sheu et al., 2010; Swartzendruber et al., 2006; Fain et al.,
258 2009). The summer maximum GOM at PDM Observatory may indicate these processes are more
259 dominant in summer than during other seasons .

260 Atmospheric GEM, PBM, and GOM displayed well-defined diel trends at PDM Observatory
261 (Figure 2). GEM concentrations (2-hour means) were relatively higher during daytime with the
262 maximum observed in the later afternoon (around 17:00) and minimum observed in the early
263 morning (around 5:00), and positively correlated with CO ($r^2 = 0.70$, $p < 0.01$). The diel trends in
264 PBM and GOM contrast with that of GEM, with the maximum PBM and GOM concentrations
265 (2-hour means) observed in the early morning (around 7:00) and the minimum concentrations in
266 the later afternoon (around 17:00) (Figure 2). PBM and GOM concentrations were significantly
267 anti-correlated with GEM concentrations ($r^2_{\text{GEM-PBM}} = 0.91$, $r^2_{\text{GEM-PBM}} = 0.87$, $p < 0.01$ for both)
268 and CO concentrations ($r^2_{\text{GEM-PBM}} = 0.74$, $r^2_{\text{GEM-PBM}} = 0.75$, $p < 0.01$ for both), and positively
269 correlated with each other ($r^2_{\text{GOM-PBM}} = 0.91$, $p < 0.01$) and with ozone concentrations ($r^2_{\text{ozone-PBM}} =$
270 0.93 , $r^2_{\text{ozone-GOM}} = 0.88$, $p < 0.01$ for both). The diel trends of atmospheric Hg species at PDM
271 Observatory were similar to those at MBO and LABS (Sheu et al., 2010; Swartzendruber et al.,
272 2006), but in contrast with the GOM diel trend at SPL which showed relatively higher values in
273 the afternoon (Fain et al., 2009). The PDM Observatory is frequently impacted by upslope, valley,
274 and plain-to-mountain breezes (Gheusi et al., 2011; Tsamalis et al., 2014). Elevated GEM
275 concentrations during daytime were likely related to upward transport of GEM enriched boundary
276 layer air, whereas elevated PBM and GOM concentrations at night were attributed to long-range
277 transport of PBM and GOM-enriched air in the free troposphere (see below).

278

279 3.2 High PBM events

280 We observed 44 high PBM events, which were defined as the peak concentrations higher than
281 31 pg m^{-3} , which are the 95th percentile PBM levels for the entire study. The maximum PBM
282 concentration was 98 pg m^{-3} , and was the highest value among the maximum PBM concentrations
283 ($33 - 40 \text{ pg m}^{-3}$) observed at high-altitude sites (Sheu et al., 2010; Swartzendruber et al., 2006; Fain
284 et al., 2009; Timonen et al., 2013).

285 For the 44 high PBM events, 30 events showed significant anti-correlations between PBM
286 and GEM concentrations (Supplementary Table S1). Also, the GEM levels during the 30 high
287 PBM events when peak PBM concentrations were observed were generally low with



288 concentrations less than the annual mean GEM concentrations of 1.86 ng m^{-3} . This phenomenon is
289 in contrast with PBM and GEM observations impacted by anthropogenic and biomass burning
290 emissions which showed simultaneous increases of PBM and GEM concentrations (Manolopoulos
291 et al., 2007; Song et al., 2009; Fu et al., 2011; Obrist et al., 2008). The air masses related to the 30
292 high PBM events mainly originated from the upper free troposphere over North America, Europe
293 and the Arctic (supplementary Figure S2). For the 30 high PBM events, 20 events had PBM/GOM
294 ratio higher than 1, indicating a significant proportion of depleted GEM in the upper free
295 troposphere was in the form of PBM rather than GOM. We acknowledge that PBM/GOM ratios
296 may be affected by bias in denuder GOM measurements (Gustin et al., 2013). Nevertheless our
297 observations on high PBM events appear different from previous studies at high-altitude sites
298 (note that these studies were conducted in the warm season or in the tropics) (Sheu et al.,
299 2010; Swartzendruber et al., 2006; Fain et al., 2009). A possible explanation is that most of the high
300 PBM events at PDM Observatory were observed in the cold season which may favor the
301 production and/or accumulation of PBM in the upper free troposphere.

302 Six out of the 44 PBM events (supplementary Table S1) were probably related to direct
303 anthropogenic pollution. These events were accompanied by elevated GEM (mean = 1.96 ± 0.13
304 ng m^{-3}) and CO concentrations (mean = 141 ± 26 ppb) and low GOM concentrations (mean = $22 \pm$
305 15 pg m^{-3}). Also, the changes in PBM concentrations, in most cases, were positively correlated
306 with GEM and CO and anti-correlated with GOM. The back trajectory analysis suggests that the
307 air masses of these 6 PBM events were likely mixed with boundary layer air over Europe prior to
308 ending at the PDM Observatory (Supplementary Figure S3). For the remaining 8 high PBM events
309 (supplementary Table S1), no significant correlations were observed between PBM concentrations
310 and GEM. However, these events were generally accompanied by typical GEM (mean = $1.76 \pm$
311 0.20 ng m^{-3}) and CO (mean = 110 ± 11 ppb) concentrations, low relative humidity (mean = $33.0 \pm$
312 24.1%), and elevated GOM concentrations (mean = $52 \pm 29 \text{ pg m}^{-3}$). Also, a significant positive
313 correlation between PBM and GOM concentrations was observed for some of these events
314 (supplementary Table S1). Therefore, these events were not likely related to direct anthropogenic
315 pollution. The air masses related to these 8 PBM events mainly originated from the middle free
316 troposphere over the North Atlantic Ocean (Supplementary Figure S4). We therefore suggest that
317 gas-particle partitioning of GOM in the middle free troposphere over the North Atlantic Ocean and
318 during long-range transport followed by mixing with European boundary layer air prior to ending
319 at PDM Observatory were the major cause for these 8 high PBM events.

320 Figure 3 shows two typical PBM events (PBM events #12 and #19 in supplementary Table
321 S1) with PBM and GEM anti-correlated. During the PBM event #12 (from 19 to 21 February 2012,
322 Figure 3A), the maximum PBM concentration reached up to 85 pg m^{-3} , which was accompanied



323 by low GEM (1.47 ng m^{-3}), low GOM (25 pg m^{-3}), low atmospheric aerosol number
324 concentrations (150 nbp cm^{-3} , Supplementary Table S1), and low relative humidity (6%) but
325 elevated CO concentration (128 ppb). The maximum PBM concentration during PBM event #19
326 was 40 pg m^{-3} (Figure 3B), which is lower than that of PBM event #12. PBM event #19 showed
327 elevated GOM concentrations (up to 131 pg m^{-3}), higher atmospheric aerosol number
328 concentration (up to 1609 nbp cm^{-3} , Supplementary Table S1) but relatively lower CO
329 concentrations (111 ppb) (Supplementary Table S1). Hysplit and Flexpart back trajectory analysis
330 shows that the air masses related to the PBM event #12 mainly originated from North America and
331 passed over high-latitude areas in the upper free troposphere prior to ending at the PDM
332 Observatory (Figure 4). PBM event #19 originated mostly from middle and upper free troposphere
333 over the Eastern North Atlantic Ocean and passed over West Europe in the middle and lower free
334 troposphere before ending at PDM Observatory (Figure 4). We find good agreement between
335 Hysplit and Flexpart in terms of air mass geographical origin and altitude over 10 days.

336 Gas-particle partitioning of GOM and heterogeneous oxidation of GEM at aerosols surfaces
337 were suggested to be two important pathways for the formation of PBM in the atmosphere
338 (Lindberg et al., 2002; Amos et al., 2012; Subir et al., 2012). For PBM event #12, direct intrusion
339 of PBM-enriched air from the upper free troposphere likely played a dominant role. PBM event
340 #19 was likely related to gas-particle partitioning of GOM generated in the middle and upper free
341 troposphere over the North Atlantic Ocean during the transport over Western Europe. The
342 mechanisms and kinetics related to production of PBM are currently not well known. In the
343 present study, we find that PBM concentrations and PBM/GOM ratios during all the events were
344 both significantly anti-correlated with the atmospheric aerosol number concentrations ($p < 0.05$,
345 Supplementary Table S2). This result indicates that concentrations of atmospheric aerosols may
346 not play a dominant role in the formation of PBM in the middle and upper free troposphere and/or
347 during the transport to the PDM Observatory, although atmospheric aerosol number
348 concentrations observed at PDM Observatory might be partially related to anthropogenic sources
349 in the boundary layer and not representative of that in the middle and upper free troposphere. On
350 the other hand, both PBM concentrations and PBM/GOM ratios during the high PBM events were
351 significantly anti-correlated with simulated mean temperature of air masses ending at the PDM
352 Observatory ($p < 0.05$ for both, Supplementary Table S2). Also, PBM/GOM ratios were found to be
353 significantly anti-correlated with simulated mean solar radiation flux ($p < 0.05$, Supplementary
354 Table S2). These results agree with previous studies which suggested that cold temperature and
355 lower winter time solar radiation enhance gas-particle partitioning of GOM and minimize the
356 decomposition of PBM by photoreduction, respectively, which in turn facilitates the accumulation
357 of PBM in the middle and upper free troposphere (Lindberg et al., 2002; Sprovieri et al.,



2005;Rutter and Schauer, 2007;Amos et al., 2012). Previous studies also suggested that aerosol uptake of atmospheric oxidants and atmospheric GEM oxidation rates may be enhanced at cold temperature(Carlaw et al., 1997;Michelsen et al., 1999;Lindberg et al., 2007), which in turn facilitates the production of PBM via heterogeneous GEM oxidation and gas-particle partitioning of GOM.

3.3 High GOM events

High GOM events were identified as the concentrations higher the 95th percentile GOM level (93 pg m⁻³) (Supplementary Table S3). For the 61 high GOM events observed, 50 events were observed with a significant anti-correlation between GOM and GEM concentrations. Also, the remaining 11 high GOM events were not likely related to direct anthropogenic pollution because GEM, CO, and atmospheric aerosol number concentrations were not elevated and no positive correlations are observed between these parameters and GOM concentrations. We therefore conclude that the high GOM events at PDM Observatory were primarily related to in situ oxidation of GEM, which is consistent with previous studies at high-altitude sites (Sheu et al., 2010;Swartzendruber et al., 2006;Fain et al., 2009).

In general, ozone, hydroxyl radical (OH·), nitrate radical (e.g. NO, NO_y), and reactive halogens (e.g. Br·, BrO, IO) are considered as potential oxidants involved in the conversion of GEM to GOM in the atmosphere (Lin and Pehkonen, 1999;Goodsite et al., 2004). However, the kinetics and relative contributions of these oxidants in the production of atmospheric GOM are not well understood. In the present study, we observed that GOM and ozone concentrations were positively correlated during 24 high GOM events (Supplementary Table S3). Meanwhile, hourly mean ozone concentrations associated with GOM peaks during the 24 high GOM events ranged from 41.4 to 98.5 ppb with an average value of 62.5 ppb, and were relatively higher than the annual mean of 49.4 ppb. The most pronounced example was observed in 16 May, 2012 (GOM Event #7, Figure 5). Clear positive correlations between GOM and ozone concentrations were also reported at MBO station, USA (Swartzendruber et al., 2006;Timonen et al., 2013), but elevated ozone concentrations as high as 105 ppb (5-min mean) during high GOM events #7 were not observed in any previous observations at high-altitude sites. The highly elevated ozone concentrations as well as low CO concentrations and relatively humidity demonstrate that event #7 was mainly related to intrusions from the upper free troposphere. This assessment was further supported by the backward trajectory analysis which shows the major origins of air masses from the upper free troposphere over the Arctic region and North America (Figure 6). At the night during event #7 when an upper tropospheric intrusion dominated, ozone concentrations were significantly anti-correlated with GEM ($GEM = -9.3 \text{ pg m}^{-3}/\text{ppb} \times O_3 \text{ ppb} + 2190 \text{ pg m}^{-3}$, $R^2 =$



393 0.72 $p < 0.01$) and positively correlated with GOM concentrations ($\text{GOM} = 2.69 \text{ pg m}^{-3}/\text{ppb} \times \text{O}_3$
394 $\text{ppb} - 113 \text{ pg m}^{-3}$, $R^2 = 0.96$, $p < 0.01$). The correlations indicated a total depletion of GEM in the
395 upper free troposphere when ozone exceeds 235 ppb, and corresponding GOM concentrations up
396 to approximately 520 pg m^{-3} . This finding is in agreement with aircraft observations of GEM and
397 GOM+PBM fractions in the upper free troposphere and tropopause (Talbot et al., 2007; Lyman and
398 Jaffe, 2012).

399 For the 24 high GOM events positively correlated with ozone, many air masses (10 out of the
400 24 high GOM events) originated from the upper troposphere over the Arctic region and the
401 remainder from the middle troposphere over the North Atlantic Ocean (Supplementary Figure S5).
402 This implies that the frequent southward intrusion of upper tropospheric air from the Arctic region
403 may be an important source of high GOM levels at PDM Observatory and mid-latitudes. In
404 general, atmospheric ozone levels exhibit a clear vertical profile with concentrations increasing
405 with altitude (Browell et al., 2003; Chevalier et al., 2007), and this may explain well the observed
406 positive correlation between GOM and ozone concentrations. However, this by no means
407 demonstrates that ozone is the exclusive oxidant during these events. In fact, nitrate radical (e.g.
408 NO , NO_y) levels were found to be tightly correlated with ozone in the upper free troposphere (Gao
409 et al., 2014; Kohler et al., 2013; Slemr et al., 2009). The vertical profiles of hydroxyl radical and
410 reactive halogens are not well established (Brune et al., 1998). However, elevated BrO and
411 OH levels were reported in the middle and upper free troposphere by previous studies (Brune et
412 al., 1998; Fittenberger et al., 2000). Therefore, these oxidants could also contribute to the
413 oxidation of GEM in the middle and upper free troposphere.

414 Nine of the high GOM events showed anti-correlations between GOM and ozone
415 concentrations (Supplementary Table S3), which are in contrast with GOM events influenced by
416 the middle and upper tropospheric air. Back trajectory analysis suggests that these events were
417 influenced by air masses originated from and/or passed over the North Atlantic in the lower free
418 troposphere (Supplementary Figure S6). This type of events was similar as that observed in the
419 Pacific Ocean MBL (Timonen et al., 2013; Laurier et al., 2003), indicating a decrease in ozone
420 concentration is a general feature of GOM production in lower free troposphere over oceans and
421 MBL. It is possible that reactive halogen and hydroxyl radicals were involved in this type of GOM
422 events, the formation of which in the MBL over oceans were thought to deplete atmospheric
423 ozone (Bloss et al., 2003; Obrist et al., 2011; Read et al., 2008).

424 High GOM events were also reported to be related to oxidation of GEM in MBL over the
425 Arctic region during Polar spring and Pacific Ocean during warm seasons (Steffen et al.,
426 2008; Timonen et al., 2013). For the high GOM events in the present study, we did not observe
427 clear evidence for the sources of GOM from the MBL over the Arctic region or the North Atlantic



428 Ocean. Therefore, the oxidation of GEM in the free troposphere was likely the predominant source
429 of high GOM at PDM Observatory. The remaining 28 high GOM events (Supplementary Table
430 S3), with GOM poorly correlated with ozone and GEM concentrations, probably reflect the
431 combined effect of intrusions of GOM-enriched air from middle and upper free troposphere, lower
432 free troposphere over the Atlantic Ocean and mixing of boundary layer air over Europe during
433 long-range transport.

434

435 **3.4 Seasonal trends of high PBM and GOM events**

436 The high PBM events were predominantly observed in winter and spring (from November to
437 April, Figure 7), which accounted for approximately 80% of the total high PBM events. In
438 contrast, high GOM events were predominantly (~69%) observed in the summer and autumn
439 (from May to October). The monthly variations in the frequencies of high PBM and GOM events
440 were consistent with the monthly means of PBM and GOM concentrations, respectively. This is
441 the first observation suggesting that high PBM and GOM events in the free troposphere in the
442 middle latitude display distinct seasonal patterns (t test: $p < 0.05$).

443 ARTs related to the high PBM events in spring and winter showed maximum values in the
444 upper free troposphere over North America (accounting for 35% of total high PBM ARTs),
445 followed by the middle free troposphere over the North Atlantic Ocean (29%), the upper free
446 troposphere over the Arctic region (22%) and the middle free troposphere over the Europe (13%)
447 (Figure 8). The maximum high PBM ARTs over North America in spring and winter were partly
448 attributed to increasing origins of air masses from this region under the influence of westerlies in
449 the mid-latitude (Figure 9). Additionally, the ratios of high PBM ARTs to total ARTs over North
450 America were also elevated in winter and spring compared to summer and spring. It is noteworthy
451 that the ratios of high PBM ARTs to total ARTs in winter and spring were significantly higher (t
452 test, $p < 0.05$) than that in summer and autumn over all the studied regions (Figure 9). This result
453 may imply that the middle and upper free troposphere of the Northern Hemisphere may be more
454 enriched in PBM in spring and winter than in summer and autumn. This conclusion is consistent
455 with the modeling result at low-altitude sites in North America which was likely due to cold
456 season subsidence of PBM enriched air from the upper troposphere and lower stratosphere (Amos
457 et al., 2012). There are currently no observations regarding the seasonal trends of atmospheric
458 PBM in the middle and upper free troposphere of the Northern Hemisphere. In spring and winter
459 increasing PBM concentrations the middle and upper free troposphere of the Northern Hemisphere
460 are apparently in contrast with the lower atmospheric aerosol concentrations observed at PDM
461 Observatory as well as other high altitudes in Europe and North America (Browell et al.,
462 2003; Asmi et al., 2011). We therefore proposed that other factors other than atmospheric aerosols



463 played a more important role in the seasonal variations of high PBM events at PDM. As we
464 discussed earlier, cold temperature and lower solar radiation may favor the production and
465 accumulation of PBM in the free troposphere. Northern Hemisphere high-latitudes are
466 characterized by relatively lower air temperature and solar radiation during the cold season, which
467 may facilitate the production and accumulation of PBM in the middle and upper troposphere in
468 cold season and explain our seasonal variations in atmospheric PBM concentrations. In summer
469 the highest residence times were observed in the lower and middle free troposphere over the North
470 Atlantic Ocean (accounting for 72% of total residence times). The lower and middle free
471 troposphere over the North Atlantic Ocean in summer produced many high GOM events (more
472 details below), which are responsible for the highest ARTs associated with high PBM events in
473 this region via gas-particle partitioning of atmospheric GOM.

474 ARTs related to the high GOM events showed maximum values over the North Atlantic
475 Ocean regardless of seasons (accounting for 62-84% of total residence times). High GOM ARTs
476 over the North Atlantic Ocean mainly correspond to the lower and middle free troposphere (Figure
477 10). In summer when most of high GOM events were observed, high GOM ARTs showed
478 maximum values in the lower free troposphere over the subtropical North Atlantic Ocean.
479 Maximum high GOM ARTs were mainly observed in the middle free troposphere over the
480 temperate and sub-arctic North Atlantic Ocean in spring and autumn (Figure 10 and 11). The
481 maximum high GOM ARTs over the subtropical North Atlantic Ocean in summer were partially
482 attributed to frequent origins of air masses from this region (Figure 11). Also, it is found that the
483 ratios of high GOM ARTs to total ARTs over the subtropical North Atlantic Ocean in summer
484 were up to an order of magnitude higher than that in other seasons over the temperate and
485 sub-arctic North Atlantic Ocean in summer. These results imply that the lower free troposphere
486 over the subtropical North Atlantic Ocean may be of specific significance for the production of
487 GOM in summer. For other seasons, the maximum high GOM ARTs over the temperate and
488 sub-arctic North Atlantic Ocean were related to frequent intrusions of air masses from the middle
489 and upper free troposphere (Figure 10 and 11).

490 The summer maximum high GOM events are also similar to observations at the Dead Sea,
491 Israel (Moore et al., 2013), which were associated with elevated BrO concentrations in the MBL.
492 Many recent studies also suggested that other oxidants such as hydroxyl radical ($\text{OH}\cdot$), iodine
493 oxides (IO), chlorine atoms (Cl \cdot), ozone, nitrogen oxides (e.g. NO_2) should be also involved in the
494 production of GOM in the atmosphere (Dibble et al., 2012; Wang et al., 2014; Weiss-Penzias et al.,
495 2015). Previous studies observed that $\text{OH}\cdot$, IO and NO_2 concentrations in the MBL and lower free
496 troposphere over the subtropical and tropical North Atlantic Ocean are highest in summer
497 (Spivakovsky et al., 2000; Savage et al., 2004; Wang et al., 2014; Martin et al., 2008), which may



498 explain the maximum summer high GOM ARTs in the lower free troposphere over the subtropical
499 North Atlantic Ocean. On the other hand, atmospheric oxidants in the middle and upper free
500 troposphere also display clear seasonal cycles. For instance, Fitzenberger et al.(2000) observed
501 that BrO concentrations in the middle and upper free troposphere over the Arctic region were
502 relatively higher in summer than in winter. Additionally, previous studies also suggested that
503 tropospheric column ozone and OH· concentrations in the Northern Hemisphere are highest in
504 summer (Spivakovsky et al., 2000;Liu et al., 2006).These oxidants may favor the in situ
505 production of GOM in the middle and upper free troposphere in summer.
506

507 **3.5 Potential source regions of PBM and GOM in different layers of troposphere**

508 The major potential source regions of PBM at PDM Observatory were located over the
509 temperate and sub-arctic North Atlantic Ocean and over Northwest Europe, whereas the major
510 potential source regions of GOM at PDM Observatory were located in the subtropical North
511 Atlantic Ocean (Figure 12). The PSCF analysis regarding the different atmospheric layers suggests
512 that major source regions of PBM and GOM were both from the middle and upper free
513 troposphere over the temperate and sub-arctic North Atlantic Ocean, Arctic region, North America,
514 and Northwest Europe, which were followed by the lower free troposphere over the subtropical
515 North Atlantic Ocean. On the other hand, the boundary layer over the Atlantic Ocean, Europe, and
516 North America played a minimal role in the sources of PBM and GOM at PDM Observatory. It
517 should be pointed out that, owing to the trailing effect (areas upwind and downwind of actual
518 source regions are likely identified as possible source regions), some of the identified source
519 regions of PBM and GOM might be overestimated. As we discussed earlier, many high PBM and
520 GOM events were related to air masses that originated from or traveled in the upper free
521 troposphere over the Arctic region and sub-arctic North America. The transport of these air masses
522 frequently took a southward route (Stohl et al., 2000), which may overestimate the contributions
523 of source regions over the temperate and sub-arctic North Atlantic Ocean and Northwest Europe.
524

525 **4 Conclusions**

526 In the present study, we consider one full year of atmospheric Hg speciation observations at
527 the high-altitude Pic du Midi (PDM) Observatory, located in the middle latitudes. Unlike previous
528 studies at other high-altitude sites (mainly conducted in warm seasons or in the tropics), we
529 observed multiple high PBM events (up to 98 pg m⁻³) in addition to multiple high GOM events
530 (up to 295 pg m⁻³), which were mainly related to in situ atmospheric transformations. The seasonal
531 variations in the occurrence of high PBM and GOM events were significantly different with most
532 of the high PBM and GOM events occurring in cold seasons (winter and spring) and warm



533 seasons (summer and autumn), respectively. Our study suggests that an important fraction of
534 depleted GEM is in the form of PBM in the middle and upper troposphere in cold seasons. These
535 findings should be taken into account by modeling approaches to better understand the fate of Hg
536 in the global atmosphere. Furthermore, our results suggest that the sources of high PBM and GOM
537 events were also different. High PBM events in cold seasons were mainly related to intrusions
538 from the upper troposphere over temperate and sub-arctic North American and Arctic regions as
539 well as the middle troposphere over the temperate North Atlantic Ocean and Europe. On the other
540 hand, high GOM events were attributed to in situ production in the middle and lower free
541 troposphere over the subtropical North Atlantic Ocean. These seasonal and regional patterns may
542 be caused by a combination of factors including variations of atmospheric oxidants and
543 meteorological parameters (e.g. temperature and solar radiation). As GOM and PBM are readily
544 deposited to Earth's surfaces, the frequent export of PBM- and GOM-enriched air from North
545 America, the Arctic region and the North Atlantic Ocean are expected to enhance wet and dry
546 deposition and cause environmental risk of mercury in European ecosystems. This should be
547 further evaluated using modeling approaches.

548

549 **Supplementary material:**

550 Tables of the identified 44 high PBM events, 61 high GOM events and Pearson's correlation
551 analysis between PBM and meteorological parameters and atmospheric pollutants are shown in
552 Tables S1-S3.

553 Time series of atmospheric Hg speciation, backward trajectories of the 30 high PBM events
554 related to upper tropospheric intrusions, backward trajectories of the 6 anthropogenic impacted
555 high PBM events, backward trajectories of the 8 mixed high PBM events, backward trajectories of
556 the 24 high GOM events related to intrusions from middle and upper troposphere, backward
557 trajectories of the 9 high GOM events related to marine free tropospheric air are shown in Figure
558 S1-S6.

559

560

561 **Acknowledgments:** This work was supported by research grant ERC-2010-StG_20091028 from
562 the European Research Council and the National Science Foundation of China (41473025,
563 41273145). We acknowledge technical support from the UMS 831 Pic du Midi observatory team.
564 Beyond mercury speciation, other observational data were provided by the PAES atmospheric
565 monitoring service supported by CNRS-INSU.

566

567 **References**

568 Amos, H. M., Jacob, D. J., Holmes, C. D., Fisher, J. A., Wang, Q., Yantosca, R. M., Corbitt, E. S.,
569 Galarneau, E., Rutter, A. P., Gustin, M. S., Steffen, A., Schauer, J. J., Graydon, J. A., St Louis, V. L.,
570 Talbot, R. W., Edgerton, E. S., Zhang, Y., and Sunderland, E. M.: Gas-particle partitioning of
571 atmospheric Hg(II) and its effect on global mercury deposition, Atmos Chem Phys, 12, 591-603, DOI



- 572 10.5194/acp-12-591-2012, 2012.
- 573 Asmi, A., Wiedensohler, A., Laj, P., Fjaeraa, A. M., Sellegri, K., Birmili, W., Weingartner, E.,
574 Baltensperger, U., Zdimal, V., Zikova, N., Putaud, J. P., Marinoni, A., Tunved, P., Hansson, H. C.,
575 Fiebig, M., Kivekas, N., Lihavainen, H., Asmi, E., Ulevicius, V., Aalto, P. P., Swietlicki, E., Kristensson,
576 A., Mihalopoulos, N., Kalivitis, N., Kalapov, I., Kiss, G., de Leeuw, G., Henzing, B., Harrison, R. M.,
577 Beddows, D., O'Dowd, C., Jennings, S. G., Flentje, H., Weinhold, K., Meinhardt, F., Ries, L., and
578 Kulmala, M.: Number size distributions and seasonality of submicron particles in Europe 2008-2009,
579 Atmos Chem Phys, 11, 5505-5538, DOI 10.5194/acp-11-5505-2011, 2011.
- 580 Bloss, W. J., Gravesstock, T. J., Heard, D. E., Ingham, T., Johnson, G. P., and Lee, J. D.: Application of a
581 compact all solid-state laser system to the in situ detection of atmospheric OH, HO₂, NO and IO by
582 laser-induced fluorescence, J Environ Monitor, 5, 21-28, Doi 10.1039/B208714f, 2003.
- 583 Browell, E. V., Hair, J. W., Butler, C. F., Grant, W. B., DeYoung, R. J., Fenn, M. A., Brackett, V. G.,
584 Clayton, M. B., Brasseur, L. A., Harper, D. B., Ridley, B. A., Klonecki, A. A., Hess, P. G., Emmons, L.
585 K., Tie, X. X., Atlas, E. L., Cantrell, C. A., Wimmers, A. J., Blake, D. R., Coffey, M. T., Hannigan, J.
586 W., Dibb, J. E., Talbot, R. W., Flocke, F., Weinheimer, A. J., Fried, A., Wert, B., Snow, J. A., and Lefer,
587 B. L.: Ozone, aerosol, potential vorticity, and trace gas trends observed at high-latitudes over North
588 America from February to May 2000, J Geophys Res-Atmos, 108, Artn 8369
589 Doi 10.1029/2001jd001390, 2003.
- 590 Brune, W. H., Faloon, I. C., Tan, D., Weinheimer, A. J., Campos, T., Ridley, B. A., Vay, S. A., Collins,
591 J. E., Sachse, G. W., Jaegle, L., and Jacob, D. J.: Airborne in-situ OH and HO₂ observations in the
592 cloud-free troposphere and lower stratosphere during SUCCESS, Geophys Res Lett, 25, 1701-1704,
593 Doi 10.1029/97gl03098, 1998.
- 594 Carslaw, K. S., Peter, T., and Clegg, S. L.: Modeling the composition of liquid stratospheric aerosols,
595 Rev Geophys, 35, 125-154, Doi 10.1029/97rg00078, 1997.
- 596 Chevalier, A., Gheusi, F., Delmas, R., Ordonez, C., Sarrat, C., Zbinden, R., Thouret, V., Athier, G., and
597 Cousin, J. M.: Influence of altitude on ozone levels and variability in the lower troposphere: a
598 ground-based study for western Europe over the period 2001-2004, Atmos Chem Phys, 7, 4311-4326,
599 2007.
- 600 Cuevas, E., Gonzalez, Y., Rodriguez, S., Guerra, J. C., Gomez-Pelaez, A. J., Alonso-Perez, S., Bustos,
601 J., and Milford, C.: Assessment of atmospheric processes driving ozone variations in the subtropical
602 North Atlantic free troposphere, Atmos Chem Phys, 13, 1973-1998, 10.5194/acp-13-1973-2013, 2013.
- 603 Dibble, T. S., Zelig, M. J., and Mao, H.: Thermodynamics of reactions of ClHg and BrHg radicals with
604 atmospherically abundant free radicals, Atmos Chem Phys, 12, 10271-10279,
605 10.5194/acp-12-10271-2012, 2012.
- 606 HYSPLIT (HYbrid Single-Particle Lagrangian Integrated Trajectory) Model access via NOAA ARL
607 READY Website (<http://www.arl.noaa.gov/HYSPLIT.php>). NOAA Air Resources Laboratory, College
608 Park, MD.
- 609 Driscoll, C. T., Mason, R. P., Chan, H. M., Jacob, D. J., and Pirrone, N.: Mercury as a Global Pollutant:
610 Sources, Pathways, and Effects, Environmental Science & Technology, 47, 4967-4983, Doi
611 10.1021/Es305071v, 2013.
- 612 Fain, X., Obrist, D., Hallar, A. G., Mccubbin, I., and Rahn, T.: High levels of reactive gaseous mercury
613 observed at a high elevation research laboratory in the Rocky Mountains, Atmos Chem Phys, 9,
614 8049-8060, 2009.
- 615 Fitzenberger, R., Bosch, H., Camy-Peyret, C., Chipperfield, M. P., Harder, H., Platt, U., Sinnhuber, B.



- 616 M., Wagner, T., and Pfeilsticker, K.: First profile measurements of tropospheric BrO, *Geophys Res Lett*,
617 27, 2921-2924, Doi 10.1029/2000gl011531, 2000.
- 618 Fu, X., Feng, X., Sommar, J., and Wang, S.: A review of studies on atmospheric mercury in China, *Sci*
619 *Total Environ*, 421-422, 73-81, 10.1016/j.scitotenv.2011.09.089, 2012.
- 620 Fu, X. W., Feng, X. B., Qiu, G. L., Shang, L. H., and Zhang, H.: Speciated atmospheric mercury and its
621 potential source in Guiyang, China, *Atmos Environ*, 45, 4205-4212, DOI
622 10.1016/j.atmosenv.2011.05.012, 2011.
- 623 Fu, X. W., Zhang, H., Yu, B., Wang, X., Lin, C. J., and Feng, X. B.: Observations of atmospheric
624 mercury in China: a critical review, *Atmos. Chem. Phys.*, 15, 9455-9476, 10.5194/acp-15-9455-2015,
625 2015.
- 626 Gao, R. S., Rosenlof, K. H., Fahey, D. W., Wennberg, P. O., Hints, E. J., and Hanisco, T. F.: OH in the
627 tropical upper troposphere and its relationships to solar radiation and reactive nitrogen, *Journal of*
628 *Atmospheric Chemistry*, 71, 55-64, DOI 10.1007/s10874-014-9280-2, 2014.
- 629 Gheusi, F., Ravetta, F., Delbarre, H., Tsamalis, C., Chevalier-Rosso, A., Leroy, C., Augustin, P., Delmas,
630 R., Ancellet, G., Athier, G., Bouchou, P., Campistron, B., Cousin, J. M., Fourmentin, M., and
631 Meyerfeld, Y.: Pic 2005, a field campaign to investigate low-tropospheric ozone variability in the
632 Pyrenees, *Atmos Res*, 101, 640-665, DOI 10.1016/j.atmosres.2011.04.014, 2011.
- 633 Goodsite, M. E., Plane, J. M. C., and Skov, H.: A theoretical study of the oxidation of Hg⁰ to HgBr₂
634 in the troposphere, *Environmental Science & Technology*, 38, 1772-1776, Doi 10.1021/Es034680s, 2004.
- 635 Gustin, M. S., Weiss-Penzias, P. S., and Peterson, C.: Investigating sources of gaseous oxidized
636 mercury in dry deposition at three sites across Florida, USA, *Atmos Chem Phys*, 12, 9201-9219,
637 10.5194/acp-12-9201-2012, 2012.
- 638 Gustin, M. S., Huang, J. Y., Miller, M. B., Peterson, C., Jaffe, D. A., Ambrose, J., Finley, B. D., Lyman,
639 S. N., Call, K., Talbot, R., Feddersen, D., Mao, H. T., and Lindberg, S. E.: Do We Understand What the
640 Mercury Speciation Instruments Are Actually Measuring? Results of RAMIX, *Environmental Science*
641 *& Technology*, 47, 7295-7306, Doi 10.1021/Es3039104, 2013.
- 642 Henne, S., Brunner, D., Folini, D., Solberg, S., Klausen, J., and Buchmann, B.: Assessment of
643 parameters describing representativeness of air quality in-situ measurement sites, *Atmos Chem Phys*,
644 10, 3561-3581, 2010.
- 645 Holmes, C. D., Jacob, D. J., Corbitt, E. S., Mao, J., Yang, X., Talbot, R., and Slemr, F.: Global
646 atmospheric model for mercury including oxidation by bromine atoms, *Atmos Chem Phys*, 10,
647 12037-12057, DOI 10.5194/acp-10-12037-2010, 2010.
- 648 Huang, J. Y., Miller, M. B., Weiss-Penzias, P., and Gustin, M. S.: Comparison of Gaseous Oxidized Hg
649 Measured by KCl-Coated Denuders, and Nylon and Cation Exchange Membranes, *Environmental*
650 *Science & Technology*, 47, 7307-7316, Doi 10.1021/Es4012349, 2013.
- 651 Kellerhals, M., Beauchamp, S., Belzer, W., Blanchard, P., Froude, F., Harvey, B., McDonald, K., Pilote,
652 M., Poissant, L., Puckett, K., Schroeder, B., Steffen, A., and Tordon, R.: Temporal and spatial
653 variability of total gaseous mercury in Canada: results from the Canadian Atmospheric Mercury
654 Measurement Network (CAMNet), *Atmos Environ*, 37, 1003-1011, Pii S1352-2310(02)00917-2
655 Doi 10.1016/S1352-2310(02)00917-2, 2003.
- 656 Kock, H. H., Bieber, E., Ebinghaus, R., Spain, T. G., and Thees, B.: Comparison of long-term trends
657 and seasonal variations of atmospheric mercury concentrations at the two European coastal monitoring
658 stations Mace Head, Ireland, and Zingst, Germany, *Atmos Environ*, 39, 7549-7556, DOI
659 10.1016/j.atmosenv.2005.02.059, 2005.



- 660 Kohler, M. O., Radel, G., Shine, K. P., Rogers, H. L., and Pyle, J. A.: Latitudinal variation of the effect
661 of aviation NO_x emissions on atmospheric ozone and methane and related climate metrics, *Atmos*
662 *Environ*, 64, 1-9, DOI 10.1016/j.atmosenv.2012.09.013, 2013.
- 663 Lan, X., Talbot, R., Castro, M., Perry, K., and Luke, W.: Seasonal and diurnal variations of atmospheric
664 mercury across the US determined from AMNet monitoring data, *Atmos Chem Phys*, 12, 10569-10582,
665 DOI 10.5194/acp-12-10569-2012, 2012.
- 666 Landis, M. S., Stevens, R. K., Schaedlich, F., and Prestbo, E. M.: Development and characterization of
667 an annular denuder methodology for the measurement of divalent inorganic reactive gaseous mercury
668 in ambient air, *Environmental Science & Technology*, 36, 3000-3009, Doi 10.1021/Es015887t, 2002.
- 669 Laurier, F. J. G., Mason, R. P., Whalin, L., and Kato, S.: Reactive gaseous mercury formation in the
670 North Pacific Ocean's marine boundary layer: A potential role of halogen chemistry, *J Geophys*
671 *Res-Atmos*, 108, Artn 4529
672 Doi 10.1029/2003jd003625, 2003.
- 673 Lee, D. S., Dollard, G. J., and Pepler, S.: Gas-phase mercury in the atmosphere of the United Kingdom,
674 *Atmos Environ*, 32, 855-864, Doi 10.1016/S1352-2310(97)00316-6, 1998.
- 675 Lin, C. J., and Pehkonen, S. O.: The chemistry of atmospheric mercury: a review, *Atmos Environ*, 33,
676 2067-2079, Doi 10.1016/S1352-2310(98)00387-2, 1999.
- 677 Lindberg, S., Bullock, R., Ebinghaus, R., Engstrom, D., Feng, X. B., Fitzgerald, W., Pirrone, N.,
678 Prestbo, E., and Seigneur, C.: A synthesis of progress and uncertainties in attributing the sources of
679 mercury in deposition, *Ambio*, 36, 19-32, 2007.
- 680 Lindberg, S. E., Brooks, S., Lin, C. J., Scott, K. J., Landis, M. S., Stevens, R. K., Goodsite, M., and
681 Richter, A.: Dynamic oxidation of gaseous mercury in the Arctic troposphere at polar sunrise,
682 *Environmental Science & Technology*, 36, 1245-1256, Doi 10.1021/Es0111941, 2002.
- 683 Liu, X., Chance, K., Sioris, C. E., Kurosu, T. P., Spurr, R. J. D., Martin, R. V., Fu, T. M., Logan, J. A.,
684 Jacob, D. J., Palmer, P. I., Newchurch, M. J., Megretskaja, I. A., and Chatfield, R. B.: First directly
685 retrieved global distribution of tropospheric column ozone from GOME: Comparison with the
686 GEOS-CHEM model, *J Geophys Res-Atmos*, 111, Artn D02308
687 Doi 10.1029/2005jd006564, 2006.
- 688 Lyman, S. N., Jaffe, D. A., and Gustin, M. S.: Release of mercury halides from KCl denuders in the
689 presence of ozone, *Atmos Chem Phys*, 10, 8197-8204, DOI 10.5194/acp-10-8197-2010, 2010.
- 690 Lyman, S. N., and Jaffe, D. A.: Formation and fate of oxidized mercury in the upper troposphere and
691 lower stratosphere, *Nat Geosci*, 5, 114-117, Doi 10.1038/Ngeo1353, 2012.
- 692 Malcolm, E. G., and Keeler, G. J.: Evidence for a sampling artifact for particulate-phase mercury in the
693 marine atmosphere, *Atmos Environ*, 41, 3352-3359, DOI 10.1016/j.atmosenv.2006.12.024, 2007.
- 694 Manolopoulos, H., Snyder, D. C., Schauer, J. J., Hill, J. S., Turner, J. R., Olson, M. L., and Krabbenhoft,
695 D. P.: Sources of speciated atmospheric mercury at a residential neighborhood impacted by industrial
696 sources, *Environmental Science & Technology*, 41, 5626-5633, Doi 10.1021/Es0700348, 2007.
- 697 Martin, M. V., Honrath, R. E., Owen, R. C., and Li, Q. B.: Seasonal variation of nitrogen oxides in the
698 central North Atlantic lower free troposphere, *J Geophys Res-Atmos*, 113, Artn D17307
699 10.1029/2007jd009688, 2008.
- 700 McClure, C. D., Jaffe, D. A., and Edgerton, E. S.: Evaluation of the KCl Denuder Method for Gaseous
701 Oxidized Mercury using HgBr₂ at an In-Service AMNet Site, *Environmental Science & Technology*,
702 48, 11437-11444, Doi 10.1021/Es502545k, 2014.
- 703 Michelsen, H. A., Spivakovsky, C. M., and Wofsy, S. C.: Aerosol-mediated partitioning of stratospheric



- 704 Cl-y and NO_y at temperatures above 200 K, *Geophys Res Lett*, 26, 299-302, Doi
705 10.1029/1998gl900281, 1999.
- 706 Moore, C. W., Obrist, D., and Luria, M.: Atmospheric mercury depletion events at the Dead Sea:
707 Spatial and temporal aspects, *Atmos Environ*, 69, 231-239, DOI 10.1016/j.atmosenv.2012.12.020,
708 2013.
- 709 Murphy, D. M., Thomson, D. S., and Mahoney, T. M. J.: In situ measurements of organics, meteoritic
710 material, mercury, and other elements in aerosols at 5 to 19 kilometers, *Science*, 282, 1664-1669, DOI
711 10.1126/science.282.5394.1664, 1998.
- 712 Murphy, D. M., Hudson, P. K., Thomson, D. S., Sheridan, P. J., and Wilson, J. C.: Observations of
713 mercury-containing aerosols, *Environmental Science & Technology*, 40, 3163-3167, Doi
714 10.1021/Es052385x, 2006.
- 715 Obrist, D., Moosmuller, H., Schurmann, R., Chen, L. W. A., and Kreidenweis, S. M.: Particulate-phase
716 and gaseous elemental mercury emissions during biomass combustion: Controlling factors and
717 correlation with particulate matter emissions, *Environmental Science & Technology*, 42, 721-727, Doi
718 10.1021/Es071279n, 2008.
- 719 Obrist, D., Tas, E., Peleg, M., Matveev, V., Fain, X., Asaf, D., and Luria, M.: Bromine-induced
720 oxidation of mercury in the mid-latitude atmosphere, *Nat Geosci*, 4, 22-26, Doi 10.1038/Ngeo1018,
721 2011.
- 722 Pirrone, N., Cinnirella, S., Feng, X., Finkelman, R. B., Friedli, H. R., Leaner, J., Mason, R., Mukherjee,
723 A. B., Stracher, G. B., Streets, D. G., and Telmer, K.: Global mercury emissions to the atmosphere from
724 anthropogenic and natural sources, *Atmos Chem Phys*, 10, 5951-5964, DOI 10.5194/acp-10-5951-2010,
725 2010.
- 726 Poirot, R. L., and Wishinski, P. R.: Visibility, Sulfate and Air-Mass History Associated with the
727 Summertime Aerosol in Northern Vermont, *Atmos Environ*, 20, 1457-1469, Doi
728 10.1016/0004-6981(86)90018-1, 1986.
- 729 Polissar, A. V., Hopke, P. K., and Harris, J. M.: Source regions for atmospheric aerosol measured at
730 Barrow, Alaska, *Environmental Science & Technology*, 35, 4214-4226, Doi 10.1021/Es0107529, 2001.
- 731 Read, K. A., Mahajan, A. S., Carpenter, L. J., Evans, M. J., Faria, B. V. E., Heard, D. E., Hopkins, J. R.,
732 Lee, J. D., Moller, S. J., Lewis, A. C., Mendes, L., McQuaid, J. B., Oetjen, H., Saiz-Lopez, A., Pilling,
733 M. J., and Plane, J. M. C.: Extensive halogen-mediated ozone destruction over the tropical Atlantic
734 Ocean, *Nature*, 453, 1232-1235, Doi 10.1038/Nature07035, 2008.
- 735 Rutter, A. P., and Schauer, J. J.: The effect of temperature on the gas-particle partitioning of reactive
736 mercury in atmospheric aerosols, *Atmos Environ*, 41, 8647-8657, DOI
737 10.1016/j.atmosenv.2007.07.024, 2007.
- 738 Savage, N. H., Law, K. S., Pyle, J. A., Richter, A., Nuss, H., and Burrows, J. P.: Using GOME NO₂
739 satellite data to examine regional differences in TOMCAT model performance, *Atmos Chem Phys*, 4,
740 1895-1912, 2004.
- 741 Schroeder, W. H., and Munthe, J.: Atmospheric mercury - An overview, *Atmos Environ*, 32, 809-822,
742 Doi 10.1016/S1352-2310(97)00293-8, 1998.
- 743 Selin, N. E., Jacob, D. J., Park, R. J., Yantosca, R. M., Strode, S., Jaegle, L., and Jaffe, D.: Chemical
744 cycling and deposition of atmospheric mercury: Global constraints from observations, *J Geophys*
745 *Res-Atmos*, 112, Artn D02308
746 Doi 10.1029/2006jd007450, 2007.
- 747 Selin, N. E., Jacob, D. J., Yantosca, R. M., Strode, S., Jaegle, L., and Sunderland, E. M.: Global 3-D



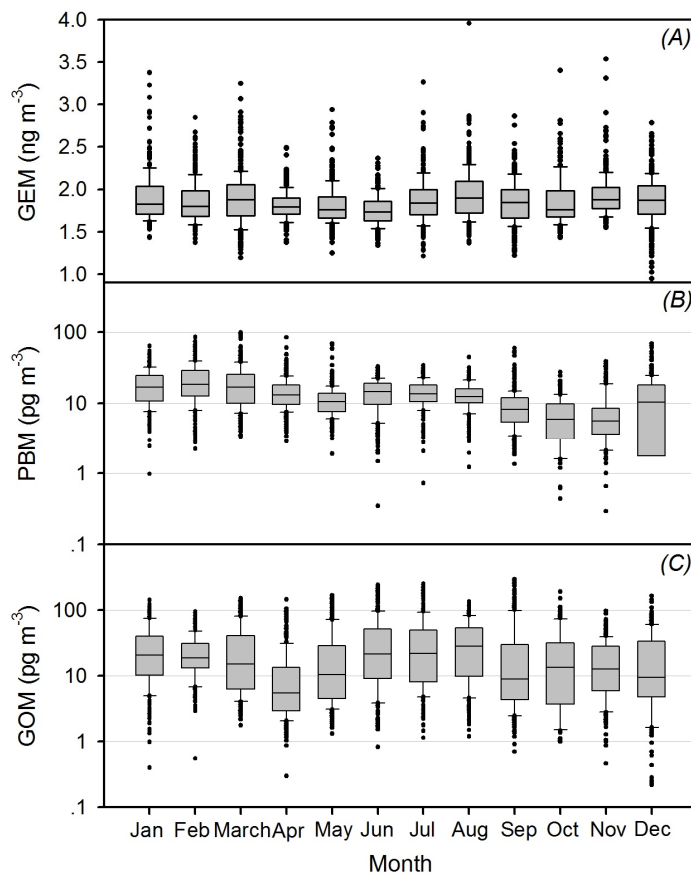
- 748 land-ocean-atmosphere model for mercury: Present-day versus preindustrial cycles and anthropogenic
749 enrichment factors for deposition, *Global Biogeochem Cy*, 22, Artn Gb2011
750 10.1029/2007gb003040, 2008.
- 751 Sheu, G. R., Lin, N. H., Wang, J. L., Lee, C. T., Yang, C. F. O., and Wang, S. H.: Temporal distribution
752 and potential sources of atmospheric mercury measured at a high-elevation background station in
753 Taiwan, *Atmos Environ*, 44, 2393-2400, DOI 10.1016/j.atmosenv.2010.04.009, 2010.
- 754 Slemr, F., and Scheel, H. E.: Trends in atmospheric mercury concentrations at the summit of the Wank
755 mountain, southern Germany, *Atmos Environ*, 32, 845-853, Doi 10.1016/S1352-2310(97)00131-3,
756 1998.
- 757 Slemr, F., Ebinghaus, R., Brenninkmeijer, C. A. M., Hermann, M., Kock, H. H., Martinsson, B. G.,
758 Schuck, T., Sprung, D., van Velthoven, P., Zahn, A., and Ziereis, H.: Gaseous mercury distribution in
759 the upper troposphere and lower stratosphere observed onboard the CARIBIC passenger aircraft,
760 *Atmos Chem Phys*, 9, 1957-1969, 2009.
- 761 Slemr, F., Weigelt, A., Ebinghaus, R., Brenninkmeijer, C., Baker, A., Schuck, T., Rauthe-Schoch, A.,
762 Riede, H., Leedham, E., Hermann, M., van Velthoven, P., Oram, D., O'Sullivan, D., Dyroff, C., Zahn,
763 A., and Ziereis, H.: Mercury Plumes in the Global Upper Troposphere Observed during Flights with the
764 CARIBIC Observatory from May 2005 until June 2013, *Atmosphere-Basel*, 5, 342-369, Doi
765 10.3390/Atmos5020342, 2014.
- 766 Song, X. J., Cheng, I., and Lu, J.: Annual atmospheric mercury species in Downtown Toronto, Canada,
767 *J Environ Monitor*, 11, 660-669, Doi 10.1039/B815435j, 2009.
- 768 Spivakovsky, C. M., Logan, J. A., Montzka, S. A., Balkanski, Y. J., Foreman-Fowler, M., Jones, D. B.
769 A., Horowitz, L. W., Fusco, A. C., Brenninkmeijer, C. A. M., Prather, M. J., Wofsy, S. C., and McElroy,
770 M. B.: Three-dimensional climatological distribution of tropospheric OH: Update and evaluation, *J*
771 *Geophys Res-Atmos*, 105, 8931-8980, Doi 10.1029/1999jd901006, 2000.
- 772 Sprovieri, F., Pirrone, N., Landis, M. S., and Stevens, R. K.: Oxidation of gaseous elemental mercury to
773 gaseous divalent mercury during 2003 polar sunrise at Ny-Alesund, *Environmental Science &*
774 *Technology*, 39, 9156-9165, Doi 10.1021/Es050965o, 2005.
- 775 Sprovieri, F., Pirrone, N., Ebinghaus, R., Kock, H., and Dommergue, A.: A review of worldwide
776 atmospheric mercury measurements, *Atmos Chem Phys*, 10, 8245-8265, DOI
777 10.5194/acp-10-8245-2010, 2010.
- 778 Steffen, A., Douglas, T., Amyot, M., Ariya, P., Aspmo, K., Berg, T., Bottenheim, J., Brooks, S., Cobbett,
779 F., Dastoor, A., Dommergue, A., Ebinghaus, R., Ferrari, C., Gardfeldt, K., Goodsite, M. E., Lean, D.,
780 Poulain, A. J., Scherz, C., Skov, H., Sommar, J., and Temme, C.: A synthesis of atmospheric mercury
781 depletion event chemistry in the atmosphere and snow, *Atmos Chem Phys*, 8, 1445-1482, 2008.
- 782 Stohl, A., Spichtinger-Rakowsky, N., Bonasoni, P., Feldmann, H., Memmesheimer, M., Scheel, H. E.,
783 Trickl, T., Hubener, S., Ringer, W., and Mandl, M.: The influence of stratospheric intrusions on alpine
784 ozone concentrations, *Atmos Environ*, 34, 1323-1354, Doi 10.1016/S1352-2310(99)00320-9, 2000.
- 785 Stohl, A., Forster, C., Frank, A., Seibert, P., and Wotawa, G.: Technical note: The Lagrangian particle
786 dispersion model FLEXPART version 6.2, *Atmos Chem Phys*, 5, 2461-2474, 2005.
- 787 Subir, M., Ariya, P. A., and Dastoor, A. P.: A review of the sources of uncertainties in atmospheric
788 mercury modeling II. Mercury surface and heterogeneous chemistry - A missing link, *Atmos Environ*,
789 46, 1-10, DOI 10.1016/j.atmosenv.2011.07.047, 2012.
- 790 Swartzendruber, P. C., Jaffe, D. A., Prestbo, E. M., Weiss-Penzias, P., Selin, N. E., Park, R., Jacob, D. J.,
791 Strode, S., and Jaegle, L.: Observations of reactive gaseous mercury in the free troposphere at the



792 Mount Bachelor Observatory, *J Geophys Res-Atmos*, 111, Artn D24302
793 Doi 10.1029/2006jd007415, 2006.
794 Talbot, R., Mao, H., Scheuer, E., Dibb, J., and Avery, M.: Total depletion of Hg degrees in the upper
795 troposphere-lower stratosphere, *Geophys Res Lett*, 34, Artn L23804
796 Doi 10.1029/2007gl031366, 2007.
797 Timonen, H., Ambrose, J. L., and Jaffe, D. A.: Oxidation of elemental Hg in anthropogenic and marine
798 airmasses, *Atmos. Chem. Phys.*, 13, 2827-2836, 10.5194/acp-13-2827-2013, 2013.
799 Tsamalis, C., Ravetta, F., Gheusi, F., Delbarre, H., and Augustin, P.: Mixing of free-tropospheric air
800 with the lowland boundary layer during anabatic transport to a high altitude station, *Atmos Res*, 143,
801 425-437, 10.1016/j.atmosres.2014.03.011, 2014.
802 Wang, F., Saiz-Lopez, A., Mahajan, A. S., Martin, J. C. G., Armstrong, D., Lemes, M., Hay, T., and
803 Prados-Roman, C.: Enhanced production of oxidised mercury over the tropical Pacific Ocean: a key
804 missing oxidation pathway, *Atmos Chem Phys*, 14, 1323-1335, 10.5194/acp-14-1323-2014, 2014.
805 Weiss-Penzias, P., Amos, H. M., Selin, N. E., Gustin, M. S., Jaffe, D. A., Obrist, D., Sheu, G. R., and
806 Giang, A.: Use of a global model to understand speciated atmospheric mercury observations at five
807 high-elevation sites (vol 15, pg 1161, 2015), *Atmos Chem Phys*, 15, 2225-2225, DOI
808 10.5194/acp-15-2225-2015, 2015.
809 Zeng, Y., and Hopke, P. K.: A Study of the Sources of Acid Precipitation in Ontario, Canada, *Atmos*
810 *Environ*, 23, 1499-1509, Doi 10.1016/0004-6981(89)90409-5, 1989.
811
812
813
814
815
816
817
818
819
820
821



822 Figure 1. Monthly variation of atmospheric GEM (A), PBM (B), and GOM (C) at PDM
823 Observatory. Box lines indicate the 10th, 25th, 50th, 75th, 90th percentiles, and data points
824 indicate concentrations below 10th and above 90th percentiles.

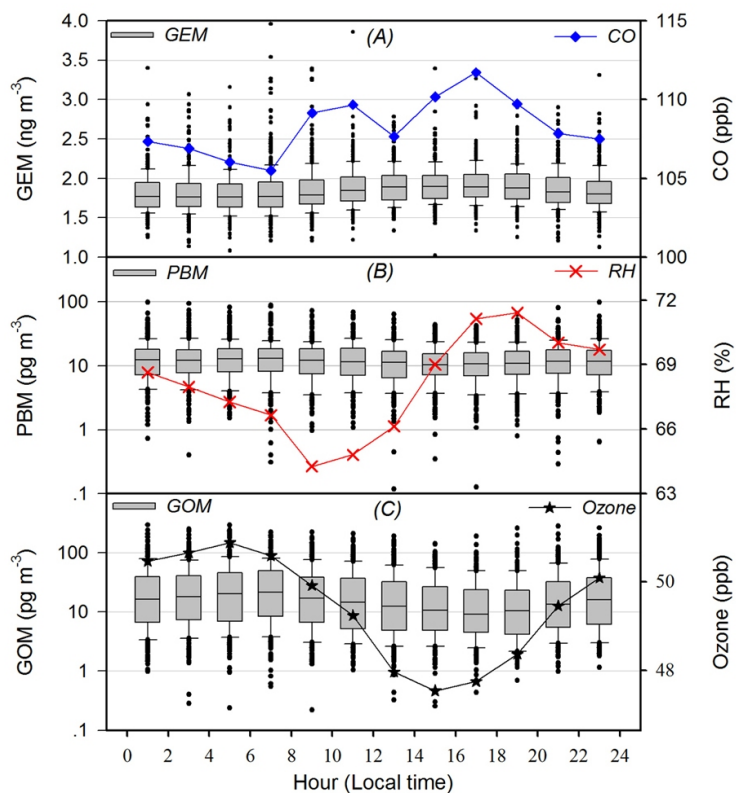


825

826



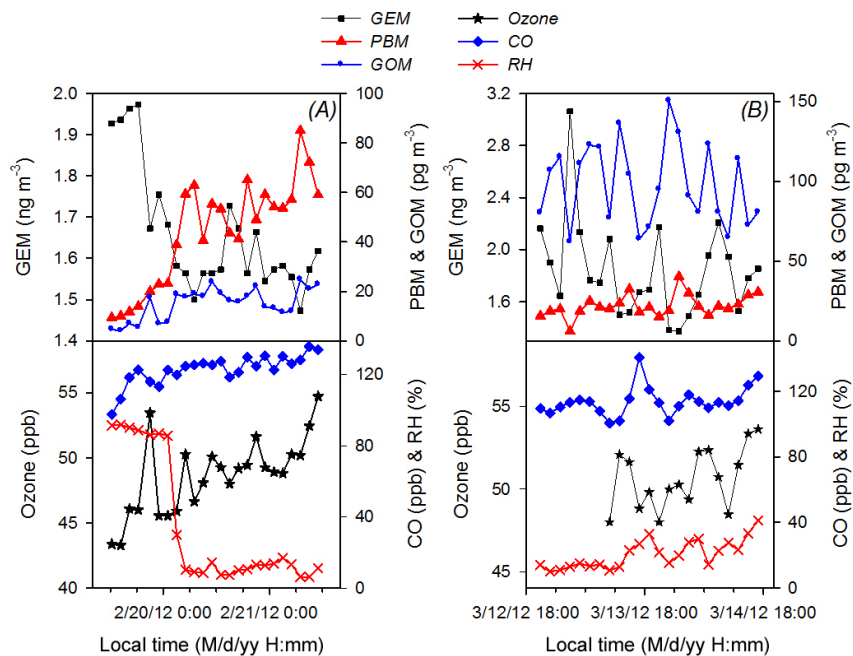
827 Figure 2. Diel, two-hour averaged, variations of atmospheric GEM and CO (A); PBM and relative
828 humidity (RH) (B); and GOM and ozone (C) at PDM Observatory. Box lines indicate the 10th,
829 25th, 50th, 75th, 90th percentiles, and data points indicate concentrations below 10th and above
830 90th percentiles.



831
832



833 Figure 3. Time series of GEM, PBM, GOM, ozone, CO, and relative humidity (RH) during high
834 PBM event #12 (A) and #19 (B).
835

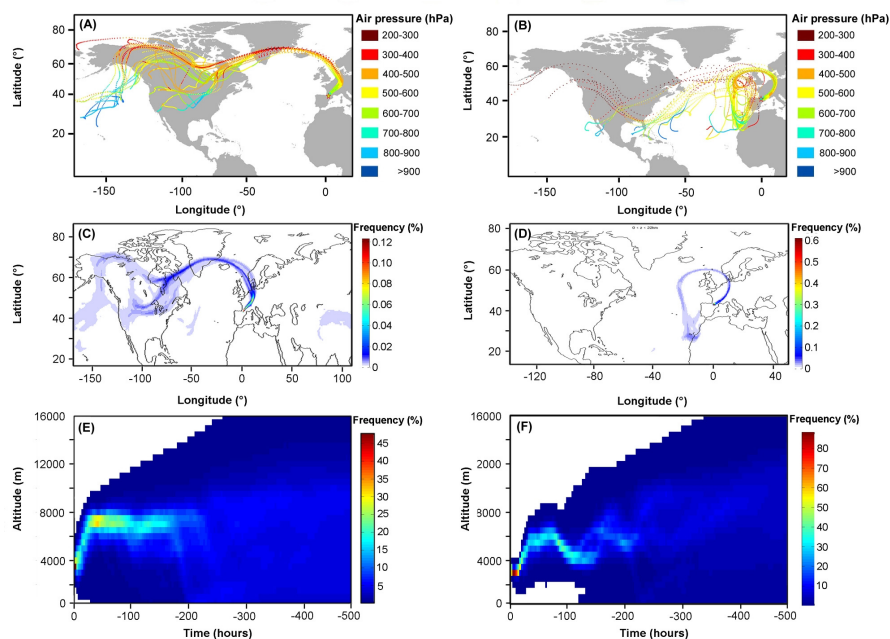


836

837



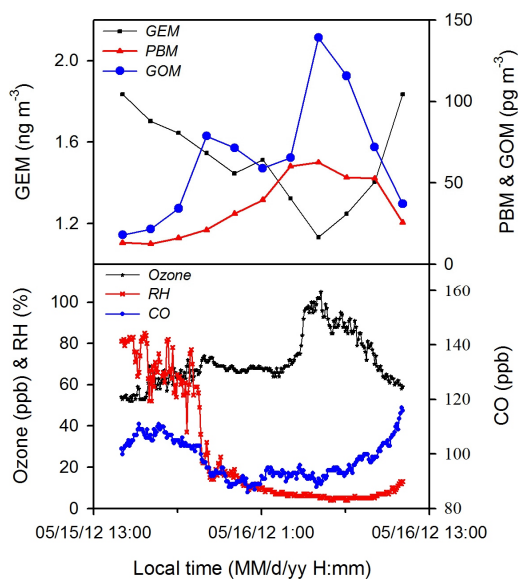
838 Figure 4. 240-h Hysplit air mass backward trajectories for the typical high PBM events #12 (A)
839 and #19 (B), Flexpart simulated air mass source regions of high PBM events #12 (C) and #19
840 (D) and Flexpart simulated air mass travelling heights of PBM events #12 (E) and #19 (F). To
841 reduce the uncertainty related to Hysplit trajectory simulations (Gustin et al., 2012), Hysplit
842 trajectories were calculated for each of the events ended at 27 locations evenly-distributed in
843 a $0.5^{\circ} \times 0.5^{\circ}$ grid cell and at a height of -500 m, 0 m, and 500 m around the PDM Observatory.



844
845



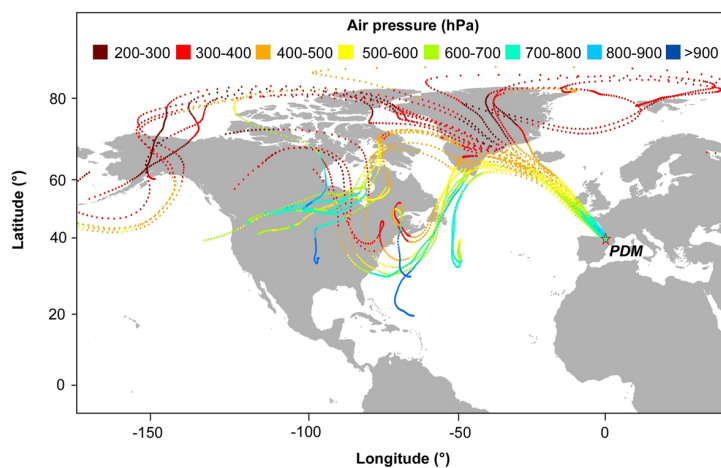
846 Figure 5. Time series of GEM, PBM, GOM, ozone, CO, and relative humidity (RH) during high
847 GOM event #7.



848
849
850
851



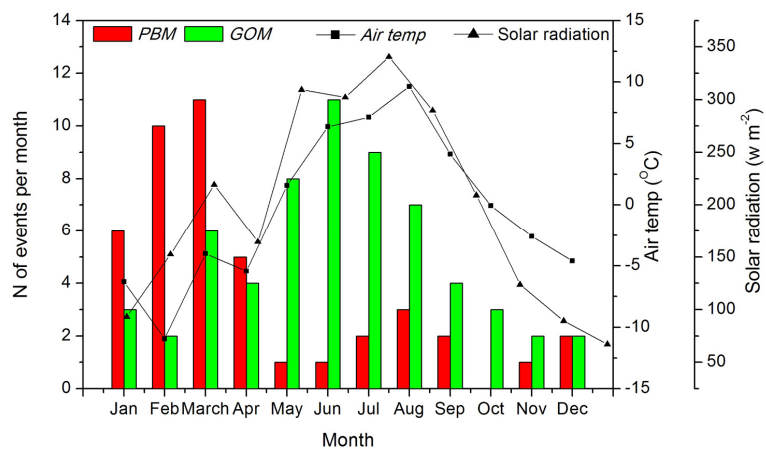
852 Figure 6. 168-h Hysplit air mass backward trajectories for the typical high GOM event #7. To
853 reduce the uncertainty related to trajectory simulations (Gustin et al., 2012), trajectories were
854 calculated for 27 locations evenly-distributed in a $0.5^\circ \times 0.5^\circ$ grid cell and at a height of -500
855 m, 0 m, and 500 m around the PDM Observatory.



856
857
858
859



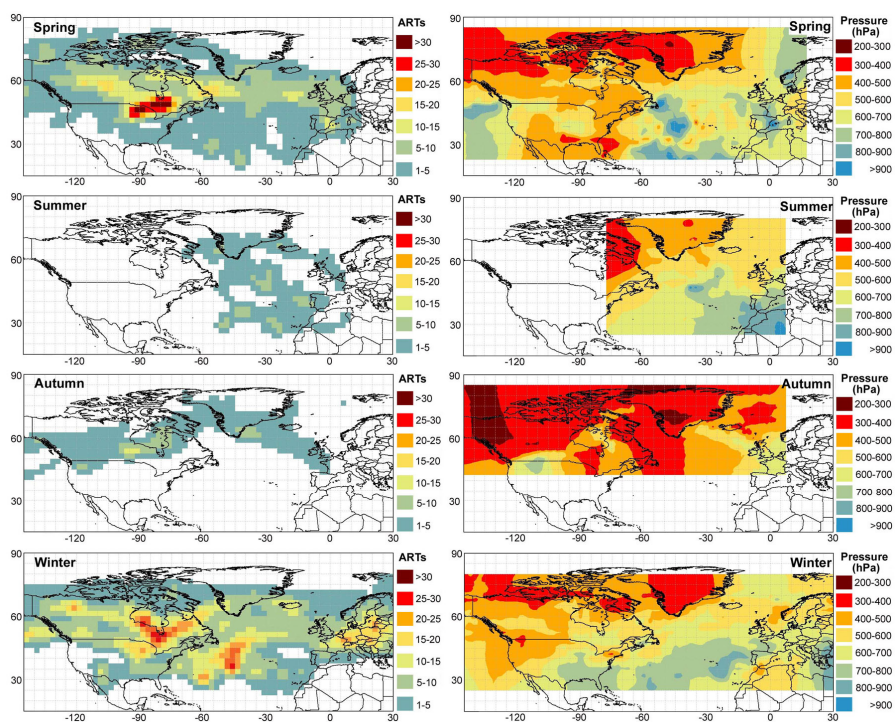
860 Figure 7. Monthly variations in the frequency of high PBM and GOM events at PDM
861 Observatory.



862
863
864
865
866



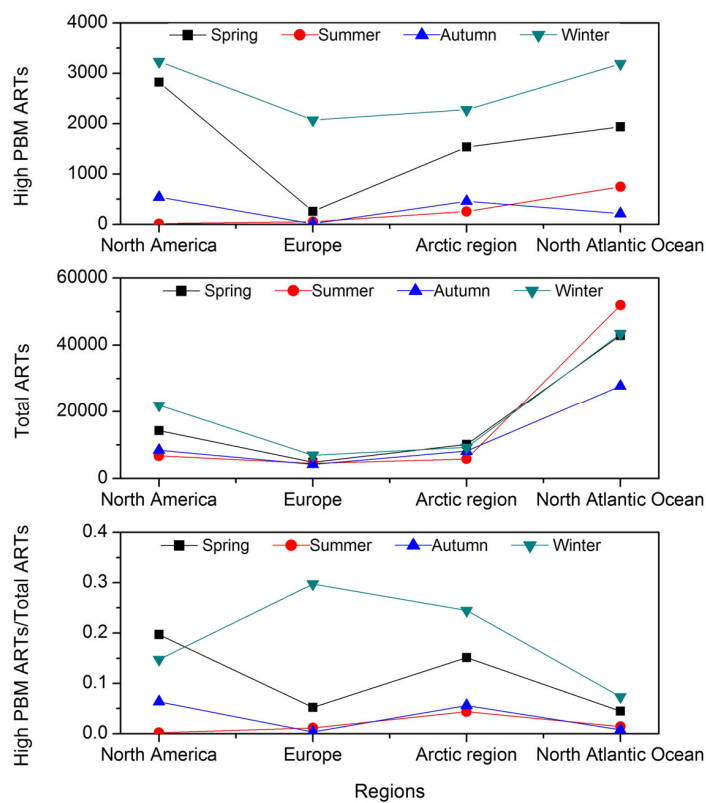
867 Figure 8. Air mass residence times (ARTs) and averaged pressure of air masses associated with
868 high PBM events for each season during the study period.



869
870
871



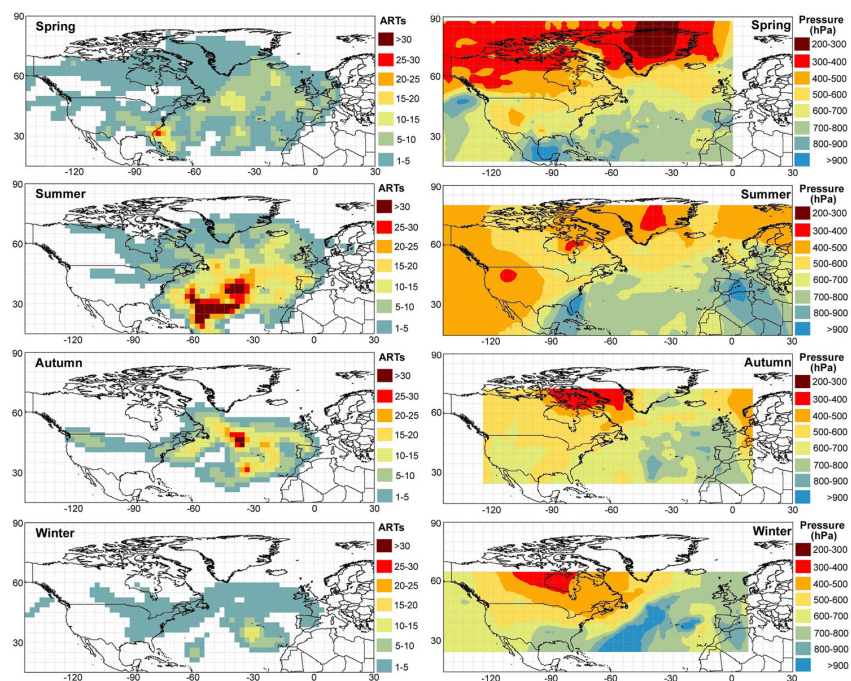
872 Figure 9. Seasonal variations in air masses residence times associated with high PBM events (high
 873 PBM ARTs, top), total residence times of all the air masses (Total ARTs, middle) and high
 874 PBM ARTs/Total ARTs ratios (bottom) in the North America, Europe, Arctic region and
 875 North Atlantic Ocean.



876
 877
 878
 879
 880
 881
 882
 883
 884
 885
 886
 887
 888
 889
 890
 891



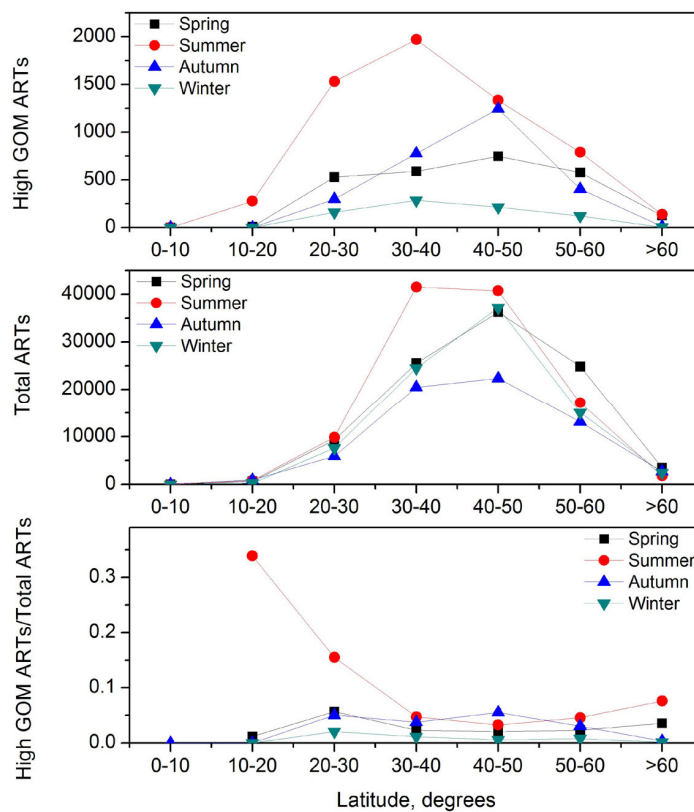
892 Figure 10. Air mass residence times (ARTs) and averaged pressure of air masses associated with
893 high GOM events for each season during the study period.



894
895
896
897



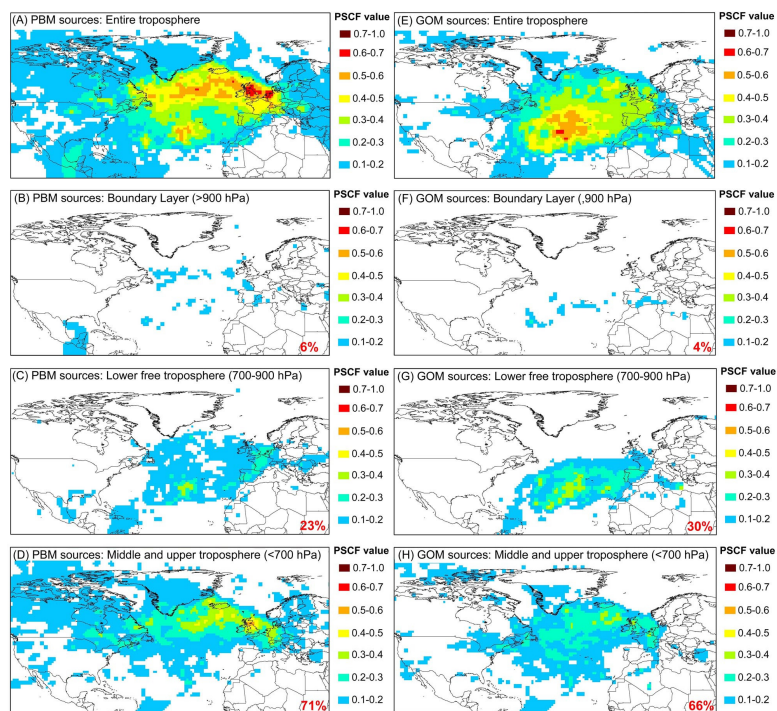
898 Figure 11. Latitude dependence of Air masses residence times (ARTs, top) associated with high
899 GOM events, total residence times of all the air masses (Total ARTs, middle) and high GOM
900 ARTs/Total ARTs ratios (bottom) over the North Atlantic Ocean for each season.



901
902
903
904



905 Figure 12. Map showing the identified potential source regions of PBM during the whole study
906 period for (A) entire troposphere, (B) boundary layer, (C) lower free troposphere, and (D)
907 middle and upper troposphere and potential source regions of GOM for (E) entire troposphere,
908 (F) boundary layer, (G) lower free troposphere, and (G) middle and upper
909 troposphere.



910